Bull. Chem. Soc. Ethiop. **2024**, 38(4), 973-988.
DOI: https://dx.doi.org/10.4314/bcse.v38i4.13

ISSN 1011-3924
Printed in Ethiopia
Online ISSN 1726-801X

THERMAL, X-RAY SPECTROSCOPY, MORPHOLOGICAL, DENSITY FUNCTIONAL THEORY AND MOLECULAR MODELING STUDIES ON YTTRIUM(III), GERMANIUM(IV), TUNGSTEN(VI), AND SILICON PENICILLINATE ANTIBIOTIC COMPLEXES

Abeer A. El-Habeeb[1*], Sonam Shakya[2], Mohamed Y. El-Sayed[3], Moamen S. Refat[4]

[1]Department of Chemistry, College of Science, Princess Nourah bint Abdulrahman University, P.O. Box 84428, Riyadh 11671, Saudi Arabia
[2]Department of Chemistry, Faculty of Science, Aligarh Muslim University, Aligarh 202002, India
[3]Chemistry Department, College of Science, Jouf University, Sakaka 2014, Saudi Arabia
[4]Department of Chemistry, College of Science, Taif University, P.O. Box 11099, Taif 21944, Saudi Arabia

(Received February 5, 2024; Revised April 2, 2024; Accepted April 4, 2024)

ABSTRACT. This manuscript elucidates the thermal stability analysis of four distinct penicillinate complexes, comprising yttrium(III), germanium(IV), tungsten(VI), and silicon, over a temperature ranging from 25 to 800°C. Thermal data revealed the high thermal stability nature of the decomposition steps. According to the spectroscopic measurements, the chemical formula of penicillinate complexes were $[Y(Pin)_2].Cl.6H_2O$ complex (**1**), $[Ge(Pin)_2].2Cl.2H_2O$ complex (**2**), $[W(Pin)_2].4Cl$ complex (**3**), and $[Si(Pin)_2].2Cl.2H_2O$ complex (**4**). The powder XRD pattern revealed crystalline to polycrystalline natures. The synthesized penicillinate complexes were subjected to theoretical calculations utilizing density functional theory (DFT) calculations, employing the lanL2DZ/6-311G++ level of theory. The optimized geometry of each penicillinate complex was discerned, and a comprehensive evaluation of various properties, including the HOMO→LUMO electronic energy gap, molecular electrostatic potential map, and additional physical parameters, was conducted and validated against experimental findings. Molecular docking tool was used to explore the anticancer activity of the synthesized penicillinate complexes in comparison with penicillin potassium drug (Pin). For the computational investigation, two kinases — CSF1R (PDB ID: 7MFC) and MEK2 (PDB ID: 1S9I) associated with breast cancer progression and estrogen-dependent breast cancer were utilized. This comprehensive analysis provides a deeper understanding of the synthesized penicillinate complexes and their potential applications.

KEY WORDS: Penicillinate complexes, TGA-DrTGA, TEM, XRD, DFT/TD-DFT, Molecular docking

INTRODUCTION

The initial investigation on metal complexes of penicillins was presented in 1957 [1-3]. The study focused on examining the interaction between potassium salts of benzylpenicillin (Bzp) and Cu^{2+} ions in aqueous solution, employing an ion exchange method [3]. The complexes $Cu(Bzp)^+$ and $Cu(Bzp)^2$ were discerned, and their respective formation constants were determined. The inference drawn from these findings posited that these complexes exhibited chelation behavior due to the coordination of the ligand (the Bzp^- anion) through the O atom of the carboxylate group and the N atom of the β-lactam group. Subsequent spectrophotometric investigations delved into the interaction of phenoxymethylpenicillin $(Fmp)^-$ with Cu(II) and Co(II) [4, 5], revealing the formation of complexes denoted as ML and ML_2. The coordination of Fmp– through the carboxylate group and the β-lactam N atom was proposed. Utilizing the AM1 and PM3 semiempirical methods, computer modeling was employed to predict potential ligand coordination in the complex of Zn(II) with the anion of a hypothetical methylpenicillin in aqueous

*Corresponding author. E-mail: aaalhabeeb@pnu.edu.sa ; dr_abeer_2@hotmail.com

solution, revealing two conceivable variants: coordination via the O atom of the carboxylate group and the N atom of the β-lactam group, or coordination through the two O atoms of the carboxylate group. Investigations detailed in [6] elucidated solid bi-ligand complexes involving Bzp– with Ni(II), Zn(II), Cd(II), Fe(III), and La(III) derived from aqueous solutions. The findings, encompassing elemental analysis of reaction products and spectroscopic analyses such as IR and EPR, concluded that in Fe(III) and La(III) complexes, ligands were coordinated via the O atoms of the carboxylate and amide groups. In Ni(II), Zn(II), and Cd(II) complexes, coordination also included the O atoms of the β-lactam group. Additionally, solid complexes of Bzp– with Fe(II) were synthesized and investigated through IR spectroscopy in [7]. These investigations elucidated the coordination of Bzp– through the carboxylate group and the β-lactam N atom. The examination of the reaction between Ni(II), Zn(II), Cd(II), Fe(III), and La(III) ions with sodium penicillinate at room temperature was conducted [8]. Two distinct classes of complexes were isolated: M(pen)2.nH2O (M = Ni(II), Zn(II), Cd(II); n = 3,4) and $M(pen)_2.Cl.nH_2O$ (M = Fe(III), La(III); n = 2). Furthermore, two unprecedented platinum(II) complexes were synthesized from the interaction of K_2PtCl_4 with penicillin V and penicillin G. The structural characterization of these complexes was accomplished through IR and NMR spectroscopy, revealing the formation of a novel, five-membered ring resulting from the chelation of the Pt^{2+} ion by the amide and thioether groups of the penicillin moiety [8]. The deprotonated form of penicillin G, as well as its complexes with Ba^{2+}, Zn^{2+}, and Cd^{2+} ions, were generated through electrospray ionization and investigated using infrared multiple photon dissociation spectroscopy coupled with Fourier-transform ion cyclotron resonance mass spectrometry. The Ba(Penicillin-H)$^+$ ion was identified as a simple complex where barium is chelated by all three carbonyl oxygens, accompanied by a cation-π interaction with the phenyl ring. The Zn(Penicillin-H)$^+$ spectrum exhibited characteristics consistent with a simple complexation in a tridentate conformation similar to that of Ba. The Cd(Penicillin-H)$^+$ complex likely adopts a simple tridentate conformation with a pronounced cation-π interaction and other metal complexes also have many applications [9]. This research article extends our prior investigation [10], wherein complexes of penicillinate with Y(III), Ge(IV), W(VI), and Si(IV) were synthesized and characterized. The current study delves into an examination of the prepared compounds, assessing their thermal stability, surface properties, particle size, and the influence of the associated metal on altering the physical characteristics of the penicillin compound.

The computational calculations were conducted utilizing the B3LYP: lanL2DZ/6-311G++ level of theory within DFT/TD-DFT (density functional theory) [11]. The analysis encompassed the optimized geometry, exploration of the molecular electrostatic potential map, and investigation of the electronic energy gap between the lowest unoccupied molecular orbital (LUMO) and highest occupied molecular orbital (HOMO) for Pin and all penicillinate complexes[$Y(Pin)_2$ complex, $Ge(Pin)_2$ complex, $W(Pin)_2$ complex, and $Si(Pin)_2$ complex]. Additionally, various crucial parameters, including chemical, structural, and spectroscopic properties, were verified.

Protein kinases, comprising a substantial enzyme family (518 in the human genome), play a vital role in catalyzing protein phosphorylation—an essential cellular mechanism governing functions like proliferation, cell cycle regulation, apoptosis, motility, growth, and differentiation. Consequently, dysregulated kinase activities are frequently associated with the initiation and progression of cancer [12]. Computational docking serves as a potent approach for comprehending and forecasting the molecular interactions between ligands and diverse biological receptors, including active sites within proteins. This intriguing protein–ligand interplay can inform the design of molecules and experimental strategies, presenting an extensive array of potential candidates for medicinal applications. For the computational investigation, we utilized two kinases — CSF1R (PDB ID: 7MFC) and MEK2 (PDB ID: 1S9I) associated with breast cancer progression and estrogen-dependent breast cancer and molecular docking tool (AutoDock Vina) was used to explore the anticancer activity of the synthesized penicillinate complexes[$Y(Pin)_2$

complex, $Ge(Pin)_2$ complex, $W(Pin)_2$ complex, and $Si(Pin)_2$ complex] in comparison with penicillin potassium drug (Pin). To gain a comprehensive understanding of the interactions, we analyzed various parameters, including binding energy, solvent-accessible surface area (SAS), interpolated charge, hydrogen bonding, aromatic, ionizability, and hydrophobic interactions at the binding sites.

EXPERIMENTAL

Synthesis of Y(III), Ge(IV), W(VI) and Si(IV) penicillinate complexes

Penicillin potassium, $YCl_3.6H_2O$, $GeCl_4$, WCl_6, and $SiCl_4$ salts were received from Sigma–Aldrich Chemical Corporation and used without further purifications. The $[Y(Pin)_2].Cl.6H_2O$ (**1**), $[Ge(Pin)_2].2Cl.2H_2O$ (**2**), $[W(Pin)_2].4Cl$ (**3**), and $[Si(Pin)_2].2Cl.2H_2O$ (**4**) complexes were prepared previously [10] with molar ratio 2:1 between penicillin potassium salt with Y(III), Ge(IV), W(VI) and Si(IV).

Analysis

Type of analysis	*Models*
Thermo gravimetric	TG/DTG–50H, Shimadzu thermo-gravimetric analyzer
SEM	Quanta FEG 250 equipment
XRD	X 'Pert PRO PANanalytical, with copper target
TEM	JEOL 100s microscopy

Density functional theory and time-dependent density functional theory (DFT and TD-DFT) studies

Density functional theory (DFT) is a quantum mechanical modeling technique widely employed in the fields of physics and chemistry. This method focuses on determining the electron density distribution within a system and utilizes this information to assess the electronic structure of atoms and molecules. By doing so, DFT provides predictions for various properties such as energy, structure, and interactions. The versatility of DFT makes it an invaluable tool for the examination of complex systems, particularly in the realms of materials science and computational chemistry. This approach plays a pivotal role in unravelling the intricate behavior and characteristics of atoms and molecules, facilitating a deeper understanding of their properties and potential applications. We employed the Gaussian 09RevD.01 package [11] for our density functional theory and time-dependent density functional theory (DFT and TD-DFT) studies. The computational calculations undertaken in this study aimed to achieve optimized molecular structures and delve into electronic transitions within Pin and all penicillinate complexes[$Y(Pin)_2$ complex, $Ge(Pin)_2$ complex, $W(Pin)_2$ complex, and $Si(Pin)_2$ complex]. Employing the B3LYP/6-311G++ basis set, a comprehensive approach amalgamating Becke's three-parameter hybrid exchange function with the Pople basis set was applied. Additionally, the Los Alamos Effective Core Potentials lanL2DZ basis set was employed specifically for the Y, Ge, W, and Si atom in the optimization process. This systematic methodology was crucial for obtaining a nuanced understanding of the molecular configurations and electronic transitions of the compounds under investigation [13]. This study encompassed a comprehensive exploration of important properties, encompassing electrostatic potential maps (MEP), the Lowest Unoccupied Molecular Orbital (LUMO), and the highest occupied molecular orbital (HOMO) for Pin and all penicillinate complexes [14]. The evaluation of frontier molecular orbitals (FMO) played a pivotal role in assessing the chemical stability of these systems. Notably, the consistently positive calculated infrared (IR) frequencies indicated

that the optimized structure represented a minimum on the potential energy surface. A meticulous assignment of bands observed in the Fourier-transform infrared (FT-IR) spectra of Pin and all penicillinate complexes was achieved through an in-depth analysis of their vibrational modes. Furthermore, our investigation extended to the computation of structure-based molecular properties in the gas phase, employing the same theoretical framework. To enhance visualization, we utilized ChemCraft 1.5 software. This multifaceted approach allowed us to derive a comprehensive understanding of the molecular characteristics and behaviors of the studied systems [15].

Molecular docking

Molecular docking stands as a pivotal computational technique within drug discovery, employed to forecast the interactions between molecules, such as small drugs and target proteins, culminating in the formation of a stable complex. This method intricately simulates the binding process, predicting the optimal orientation and conformation of the molecules in relation to the target protein. Through a thorough assessment of energetics and geometric complementarity, molecular docking provides estimations of binding affinity, shedding light on the strength of the interaction. The utility of docking extends to the identification of potential drug candidates, offering insights into their intricate interactions with specific protein targets. Moreover, it serves as a valuable tool in the strategic design and optimization of novel pharmaceuticals. The application of molecular docking in drug discovery is instrumental in expediting the identification and development of promising therapeutic agents. In this study, the entire docking experiment was executed on a processor with the following specifications: Intel(R) Core(TM) i5-4200U CPU @ 1.60 GHz, 2.10 GHz, 2.30 GHz, 64-bit architecture.

The initial molecular structure of all penicillinate complexes [$Y(Pin)_2$ complex, $Ge(Pin)_2$ complex, $W(Pin)_2$ complex, and $Si(Pin)_2$ complex]and Pin drug, which had been optimized through DFT calculations, served as our starting structures. The conversion of these molecular structures into PDBQT format was facilitated through the utilization of OpenBabelIGUI software, version 2.4.1 [16, 17], which can be accessed at http://openbabel.org/wiki/Main_Page. Structural data for the two potential kinases, namely CSF1R (PDB ID: 7MFC) and MEK2 (PDB ID: 1S9I), were retrieved from the RCSB Protein Data Bank online [18]. Following this, we meticulously prepared the receptors for the subsequent docking process by removing the native ligands and any other heteroatoms, including water molecules, utilizing BIOVIA Discovery Studio (DS) Visualizer (v19.1.0.18287). To enhance accuracy, the receptor structures were augmented with polar hydrogen atoms, and Kollman charges were determined using Autodock Tool [19]. The assignment of partial charges adhered to the Geistenger method. Subsequently, the final docking of receptors and ligands (comprising all penicillinate complexes and the Pin drug) was executed using Autodock Vina [20]. The resulting docked poses underwent meticulous scrutiny to evaluate the interactions, with a comprehensive analysis conducted using DS Visualizer, accessible at https://www.3ds.com/products-services/biovia/. This systematic approach ensured the precision and reliability of the molecular docking process, allowing for a detailed exploration of the interactions between receptors and ligands.

RESULTS AND DISCUSSION

Thermogravimetric analyses

The TGA curves (Figure 1) of the penicillinate potassium drug and its Y(III), Ge(IV), W(VI), and Si(IV) penicillinate complexes have been assigned. The hydrated penicillinate complexes of $[Y(pin)_2].Cl.6H_2O$ (**1**), $[Ge(pin)_2].2Cl.2H_2O$ (**2**) and $[Si(pin)_2].2Cl.2H_2O$ (**4**) are loss of hydrated water molecules at first decomposition step within temperature range of 58-124, 150-202 and 99-

142 °C at maximum differential thermogravimetric analysis at 87, 163 and 115 °C, respectively. The anhydrous [W(pin)$_2$].4Cl (**3**) complex is stable up to 200-700 °C. The TGA-DrTGA curves of yittrium(III), germanium(IV), tungsten(VI) and silicon(IV) complexes refer to thermal decomposition in three-to-five degradation steps at DTG_{max} = (87, 255 and 519°C), (163, 268, 311, 380 and 493 °C) and (189, 299, 467 and 667 °C) and (115, 198, 263 and 525 °C), respectively. These peaks are endothermic attributed to the pyrolysis of two penicillinate molecules. At these DTG_{max} stages, the weight losses of the respected four penicillinate complexes are 71.917, 74.190, 79.659. and 91.604% from the original sample weight. The residual materials correspond to metallic oxides polluted with few carbon atoms.

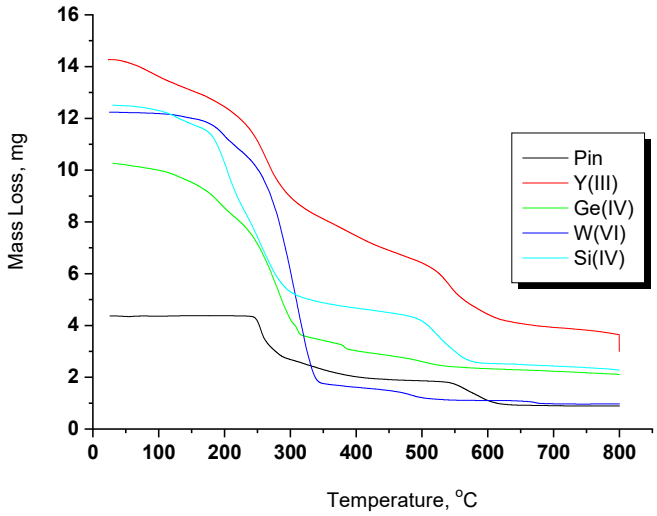

Figure 1. TGA curves of penicillinate complexes.

Morphological studies (XRD, SEM, and TEM)

XRD patterns of penicillinate complexes have a crystalline to semi-crystalline nature as shown in Figure 2a-d. The observed peaks corresponded respectively to the single-phase cubic semi-crystalline yttrium nano-particles (Figure 2a) came in agreement with the JCPDS 41-1105 reference [21], the data recorded from main peaks at 2θ = 27.81, 32.56 and 52.75°. The X-ray diffraction spectrum of germanium complex is shown in Figure 2b and has distinguished peaks at 32.52, 46.70, 58.28 and 77.58° due to the conformation about presence of Ge metal in the construction of complex [22, 23]. Regarding tungsten(VI) penicillinate complex, three reflection peaks at 2θ = 40.06, 58.25, and 77.86° correspond to (110), (200) and (211) planes of tungsten metal [24]. XRD of the silicon(IV) complex has three strongest diffraction peaks at 2θ = 28.26, 49.96, and 58.41°. The XRD results showed that penicillinate complexes of [Y(pin)$_2$].Cl.6H$_2$O (**1**), [Ge(pin)$_2$].2Cl.2H$_2$O (**2**), [W(pin)$_2$] (**3**) and [Si(pin)$_2$].2Cl .2H$_2$O (**4**) have presumably a better degree of crystallinity, as shown in Figure 2. The crystallite sizes were determined by means of the Scherrer equation [25]. The average of crystallite sizes of the penicillinate complexes present at 48.78, 85.94, 82.31, and 95.82 nm for the yittrium(III), germanium(IV), tungsten(VI) and silicon(IV) complexes, respectively, according to the estimation of all distinguish peaks.

SEM images are shown in Figure 3a-d, its shows a homogeneous surface morphologically for the penicillinate complexes. The particle size of synthesized complexes is within 5-50 µm with different magnification ranges between X500-X3000.

TEM images (Figure 3a-d) of the penicillinate complexes show particles within a nano- scale range. The average particle diameter for these complexes was determined by adjusting the data obtained from the TEM micrograph. The dark spot spherical particle sizes were inserted within the 50-100 nm range in agreement with the XRD estimate.

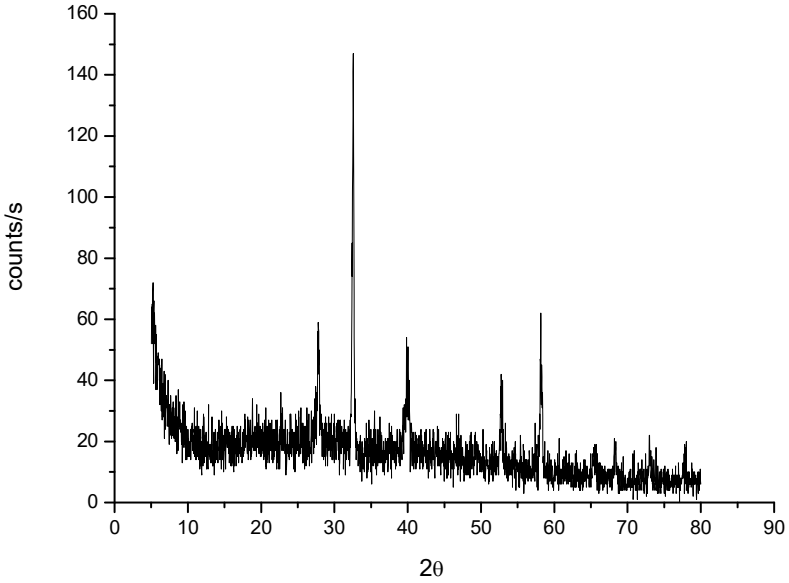

Figure 2a. XRD patterns of $[Y(pin)_2].Cl.6H_2O$ complex.

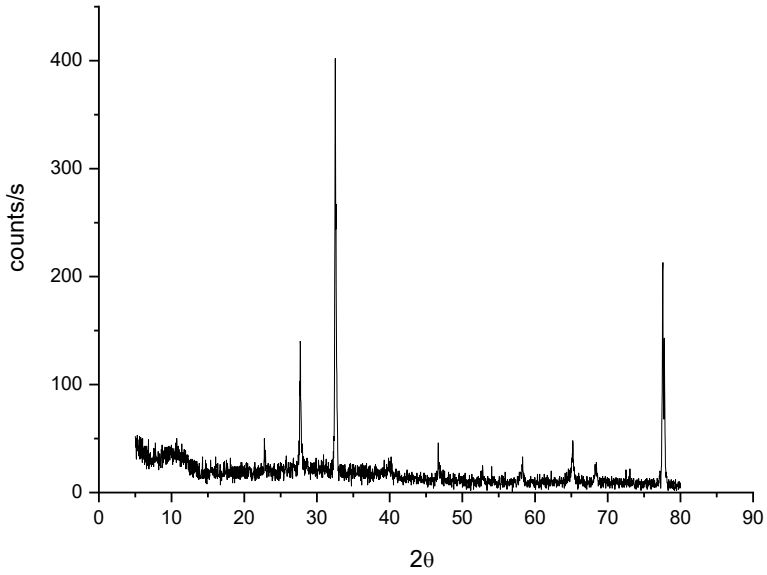

Figure 2b. XRD patterns of $[Ge(pin)_2].2Cl.2H_2O$ complex.

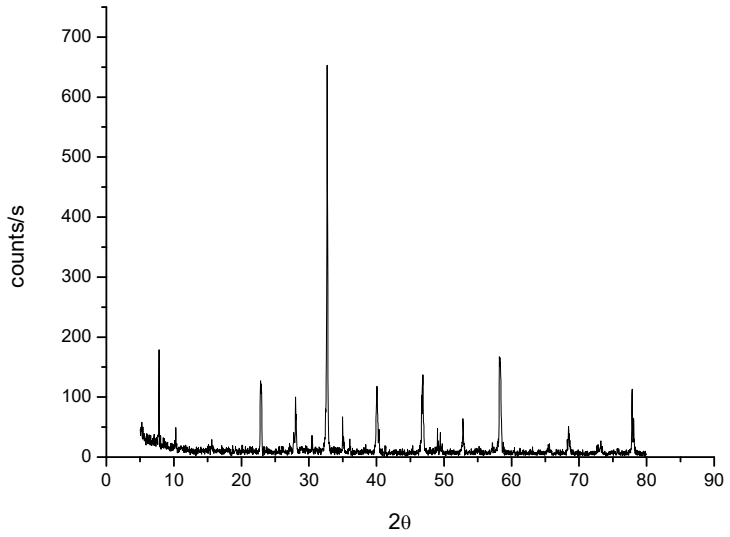

Figure 2c. XRD patterns of $[W(pin)_2].4Cl$ complex.

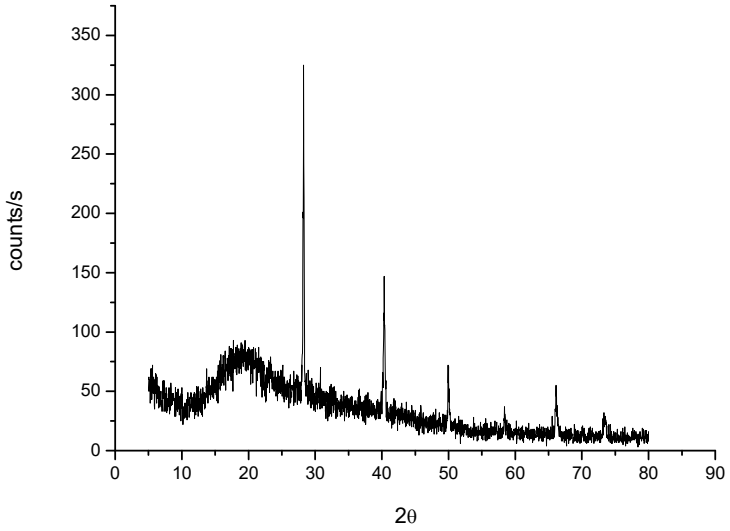

Figure 2d. XRD patterns of $[Si(pin)_2].2Cl.2H_2O$ complex.

Density functional theory calculations

We utilized the B3LYP: lanL2DZ / 6-311G++ level of theory to obtain optimized structures for all penicillinate complexes [$Y(Pin)_2$ complex, $Ge(Pin)_2$ complex, $W(Pin)_2$ complex, and $Si(Pin)_2$ complex]and Pin drug. The minimum SCF energy for Pin, $Y(Pin)_2$ complex, $Ge(Pin)_2$ complex, $W(Pin)_2$ complex, and $Si(Pin)_2$ complex was calculated to be -1068.50747, -2091.11429, -2058.07086, -2122.50332, and -2058.26070 atomic units after 21, 56, 41.59, and 53 optimization

steps, respectively [26]. The optimized geometries, including atomic coordinates and strain-free lattice constants for all penicillinate complexes [$Y(Pin)_2$ complex, $Ge(Pin)_2$ complex, $W(Pin)_2$ complex, and $Si(Pin)_2$ complex] and pin drug are presented in Figure 4. Electrostatic potential strengths for all penicillinate complexes [$Y(Pin)_2$ complex, $Ge(Pin)_2$ complex, $W(Pin)_2$ complex, and $Si(Pin)_2$ complex] and pin drug are depicted in the Molecular Electrostatic Potential (MEP) maps. Electropositive regions are represented in blue, while electronegative regions are in red. These maps reveal preferential binding sites for electrophilic and nucleophilic interactions over the molecules [27]. The MEP surface map is presented on a color scale ranging from deep red to deep blue, which is -8.451 e-2 to +8.451 e-2 for Pin, -6.918 e-2 to +6.918 e-2 for $Y(Pin)_2$ complex, -4.958 e-2 to +4.958 e-2 for $Ge(Pin)_2$ complex, -5.248 e-2 to +5.248 e-2 for $W(Pin)_2$ complex, and -5.539 e-2 to +5.539 e-2 for $Si(Pin)_2$ complex [28].

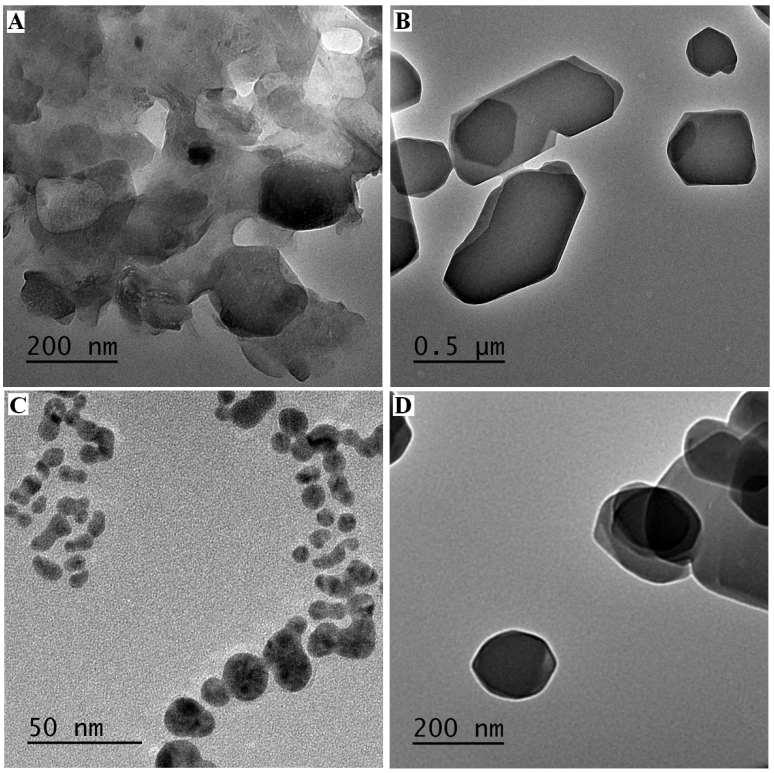

Figure 3. TEM morphology of (a) yttrium(III), (b) germanium(IV), (c) tungsten(VI) and (d) silicon(IV) penicillinate complexes.

We investigated the IR spectra of Pin drug and all penicillinate complexes [$Y(Pin)_2$ complex, $Ge(Pin)_2$ complex, $W(Pin)_2$ complex, and $Si(Pin)_2$ complex]in the gas phase using the DFT approach at the B3LYP/LanL2DZ level of theory to complement the experimental findings. The simulated spectra for Pin drug, $Y(Pin)_2$ complex, $Ge(Pin)_2$ complex, $W(Pin)_2$ complex, and $Si(Pin)_2$ complex, scaled at 0.9601, 0.9824, 0.9241, 0.9302, and 9369, respectively. Several significant vibrational signals observed in the experimental FTIR spectrum align well with the simulated IR spectrum, as confirmed through animated modes [29]. For free Pin drug, the IR

spectrum reveals bands at 3483 cm^{-1}, corresponding to the N-H vibrations. Aromatic and aliphatic C-H vibrations appear at 3086 and 2920 cm^{-1}, respectively, while the C=O stretching vibration is observed at 1694 cm^{-1}. The band at 1597 and 1487 cm^{-1} attributed to the *ν*(N-H) vibration.

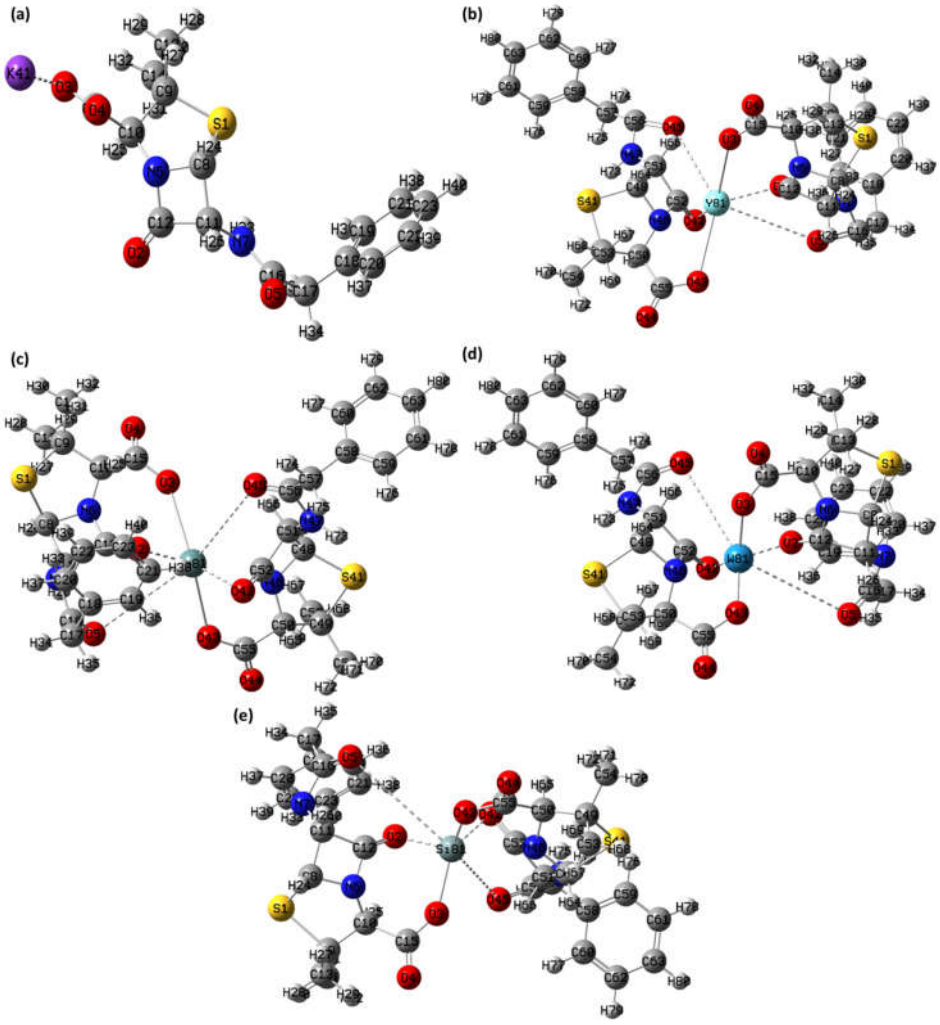

Figure 4. Optimized structure of (a) Pin, (b) $Y(Pin)_2$ complex, (c) $Ge(Pin)_2$ complex, (d) $Ge(Pin)_2$ complex, and (e) $Si(Pin)_2$ complex with Mulliken atom numbering scheme.

Similarly, for $Y(Pin)_2$ complex, $Ge(Pin)_2$ complex, $W(Pin)_2$ complex, and $Si(Pin)_2$ complex, the N-H vibration is prominent at 3499, 3492, 3489, and 3497 cm^{-1}, respectively. Aromatic C-H vibrations are observed at 3256, 3214, 3261, and 3259 cm^{-1} for $Y(Pin)_2$ complex, $Ge(Pin)_2$ complex, $W(Pin)_2$ complex, and $Si(Pin)_2$ complex, respectively. Aliphatic C-H vibrations are observed at 3051, 3080, 3067, and 3047 cm^{-1} for $Y(Pin)_2$ complex, $Ge(Pin)_2$ complex, $W(Pin)_2$ complex, and $Si(Pin)_2$ complex, respectively, while C=O vibrations occur at 1775, 1773, 1726,

and 1695 cm^{-1} for $Y(Pin)_2$ complex, $Ge(Pin)_2$ complex, $W(Pin)_2$ complex, and $Si(Pin)_2$ complex, respectively. Some deviation from experimental data is expected due to the simplifications and anharmonicity of the basis set; hence, a scaling factor was applied to align the simulated and experimental vibrational frequencies [30].

We have also examined the electronic transitions of Pin drug, $Y(Pin)_2$ complex, $Ge(Pin)_2$ complex, $W(Pin)_2$ complex, and $Si(Pin)_2$ complex in the gas phase using the TD-DFT method. TD-DFT results showed electronic absorption bands for Pin drug, $Y(Pin)_2$ complex, $Ge(Pin)_2$ complex, $W(Pin)_2$ complex, and $Si(Pin)_2$ complex at 265, 368, 356, 342, and 316 nm [31]. Figure 5 illustrates the spatial arrangements of HOMO and LUMO, along with the HOMO-LUMO gap for Pin drug, $Y(Pin)_2$ complex, $Ge(Pin)_2$ complex, $W(Pin)_2$ complex, and $Si(Pin)_2$ complex. The HOMO to LUMO gap (ΔE) was found to be 4.6795, 3.3693, 3.4827, 3.6252, and 3.9235 eV for Pin drug, $Y(Pin)_2$ complex, $Ge(Pin)_2$ complex, $W(Pin)_2$ complex, and $Si(Pin)_2$ complex, respectively [32]. This energy gap correlates with the chemical stability of the molecules. Smaller energy gaps indicate higher chemical reactivity, lower kinetic stability, and a softer nature, whereas larger energy gaps suggest the opposite. On the basis of the energy gap, the order of stability is as follows - $Y(Pin)_2$ complex >$Ge(Pin)_2$ complex > $W(Pin)_2$ complex > $Si(Pin)_2$ complex >Pin drug. We have tabulated some molecular parameters in Table 1, derived from the gas-phase analysis, HOMO-LUMO properties, and optimized geometries [33].

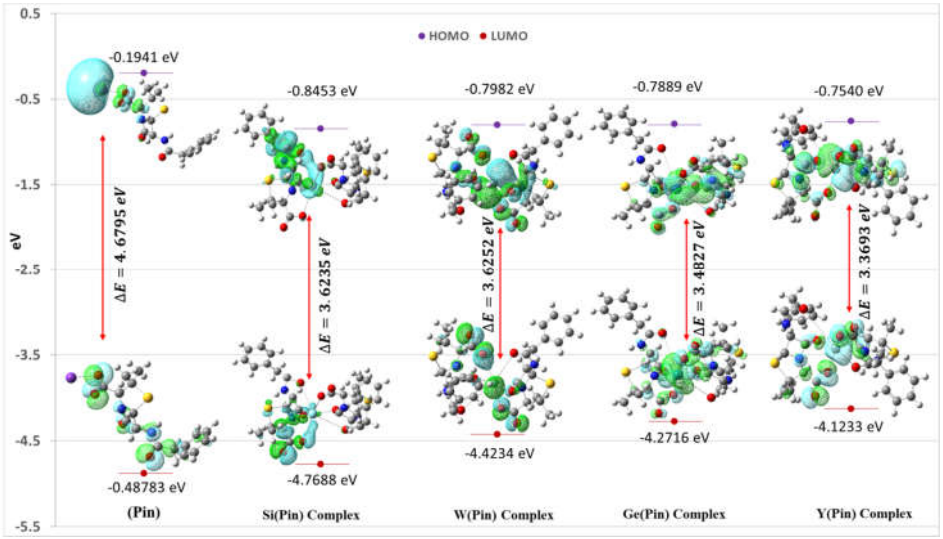

Figure 5. Spatial plot of HOMO and LUMO with their energy gap for Pin, $Y(Pin)_2$ complex, $Ge(Pin)_2$ complex, $Ge(Pin)_2$ complex, and $Si(Pin)_2$ complex.

Molecular docking studies

To better elucidate the inhibitory properties of our all penicillinate complexes [$Y(Pin)_2$ complex, $Ge(Pin)_2$ complex, $W(Pin)_2$ complex, and $Si(Pin)_2$ complex] as an anticancer agent, we have screening two potential kinases (CSF1R and MEK2) implicated in tumorigenesis, based on the 2020 FDA-approved small molecule protein kinase inhibitors [34]. This screening is performed by a molecular docking approach (see experimental part). It has been reported that high expression of CSF1R is related to breast cancer progression [35, 36] and expression of MEK2 pathway activity was linked to estrogen-dependent breast cancer [37].

Table 1. Various other theoretical molecular parameters of Pin and synthesized penicillinate complexes.

Parameters	RB3LYP/lanL2DZ				
	Pin	$Y(Pin)_2$ complex	$Ge(Pin)_2$ complex	$W(Pin)_2$ complex	$Si(Pin)_2$ complex
Minimum SCF energy (a.u.)	-1068.50747	-2091.11429	-2058.07086	-2122.50332	-2058.26070
Polarizability (α) (a.u.)	209.671854	748.642006	402.859585	343.580319	3.476670
Dipole Moment (Debye)	11.962336	9.883003	5.013540	1.482934	3.476670
Zero point vibrational energy (kcal/mol)	411.80480	407.89901	409.77471	413.42388	413.4125
Total thermal energy (kcal/mol)	212.054	425.857	434.772	439.770	436.714
Electronic spatial extent (a.u.)	11935.2455	36329.6692	35887.6416	33800.0661	35174.4167
Frontier MO energies (eV)					
LUMO	-0.1941	-0.7540	-0.7889	-0.7982	-0.8453
HOMO	-4.8783	-4.1233	-4.2716	-4.4234	-4.7688
Gap (HOMO – LUMO)	4.6795	3.3693	3.4827	3.6252	3.9235

We conducted molecular docking studies of Pin drug, $Y(Pin)_2$ complex, $Ge(Pin)_2$ complex, $W(Pin)_2$ complex, and $Si(Pin)_2$ complex with the prepared kinases — CSF1R (PDB ID: 7MFC) and MEK2 (PDB ID: 1S9I). Subsequently, we identified the most favorable docking poses. To assess the relative efficiency of Pin drug compared all penicillinate complexes, we performed a theoretical comparison. Molecular docking results show that the potential energy of binding of all penicillinate complexes is higher than that of Pin drug for both kinases (see Table 2). Notably, $Y(Pin)_2$ complex exhibited the highest docking energy value when interacting with CSF1R, with a potential binding energy of 11.6 kcal/mol. The higher binding energy value of $Y(Pin)_2$ complex with CSF1R signifies a stronger interaction as compared with others. The best docking pose Pin drug and all penicillinate complexes with CSF1R and with MEK2 are included in Table 3 which provides the other important data related to docking. These results shows a strong binding of $Y(Pin)_2$ complex with both the kinases (CSF1R and MEK2) among all penicillinate complexes and including Pin drug. A 3D and 2D depiction of the molecular docking representation for the interactions between ligands and receptors was provided in Figures 6. As shown in Figure 6, Pin with CSF1R reveals the amino acid residues, His776 shows π - π stacked interaction. Additionally, Leu769 and Ile646 show π-Alkylinteraction [38, 39]. On the other hand$Y(Pin)_2$ complex with CSF1R forms hydrogen bond with Arg777, including attractive charge interaction. Additionally, Glu628 as amide - π stacked, Ile363 and Ile803 as alkyl, and Tyr809, Ala639, and Ala815 as π-Alkyl interaction are also present. These findings suggest that the synthesized $Y(Pin)_2$ complex exhibits more efficient binding with both kinases, especially with CSF1R.

Table 2. The docking score of Pin and synthesized penicillinate complexes docked with two kinases — CSF1R (PDB ID: 7MFC) and MEK2 (PDB ID: 1S9I).

S. No.	Ligand	Binding free energy (kcal/mol)	
		PDB ID: 7MFC	PDB ID: 1S9I
1	Pin	-7.1	-8.1
2	$Y(Pin)_2$ complex	-11.6	-11.0
3	$Ge(Pin)_2$ complex	-9.5	-9.4
4	$W(Pin)_2$ complex	-9.2	-9.4
5	$Si(Pin)_2$ complex	-9.4	-10.7

Table 3. The interactions of CSF1R with Pin drug and synthesized penicillinate complexes.

S. No.	Ligand+Receptor	Interactions	
		H-Bond	Others
1	Pin+ CSF1R	-	His776 (π - π stacked);Leu769 and Ile646 (π-Alkyl)
2	$Y(Pin)_2$ complex+ CSF1R	Arg777	Glu628 (amide - π stacked); Ile363 and Ile803 (alky); and Tyr809, Ala639, and Ala815 (π-Alkyl)
3	$Ge(Pin)_2$ complex + CSF1R	Try668	Phe797 (π- π T-shaped); Arg677 (Alkyl); Leu588 and Arg801 (π-Alkyl)
4	$W(Pin)_2$ complex + NF-kB	Asn673 and Try668	Asp670 (π-Anion); Phe797 (π- π T-shaped); Leu588 (π-Sigma); Arg677 (Alkyl)
5	$Si(Pin)_2$ complex +CSF1R	-	Met637 (π-Sulfur); Phe593 (π- π T-shaped); Pro818 (Alkyl); Try809 and Ala629 (π-Alkyl)

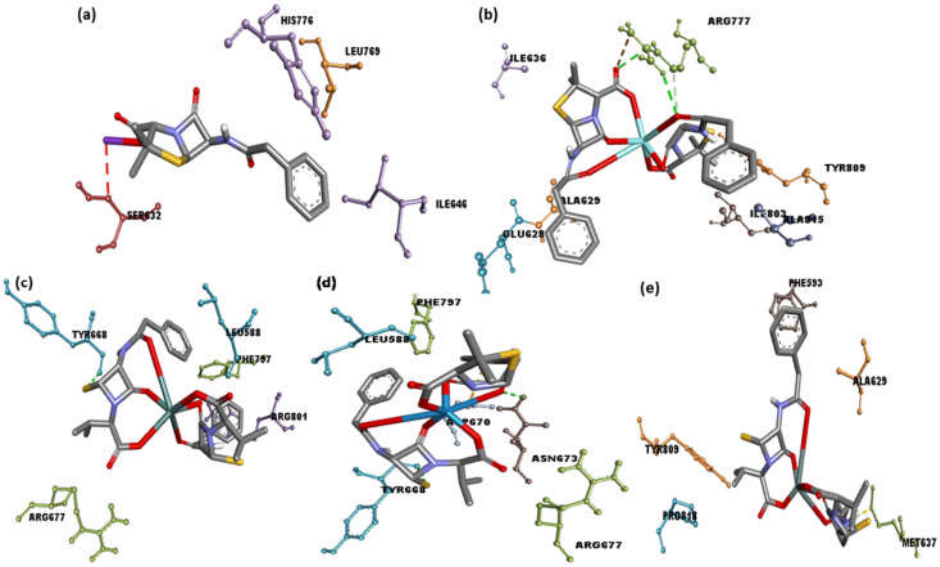

Figure 6. 3D representation of interactions for CSF1R (PDB ID: 7MFC) docked with (a) Pin, (b) $Y(Pin)_2$ complex, (c) $Ge(Pin)_2$ complex, (d) $Ge(Pin)_2$ complex, and (e) $Si(Pin)_2$ complex.

Aromatic, hydrophobicity, hydrogen bond, SAS, interpolated charge, and ionizability surfaces study

We analyzed the docking results using the Discovery Studio (DS) software, which allowed us to visualize various surfaces around the ligand and the receptor's interaction site [38]. In Figure 7, we present graphical representations of aromatic surface, interpolated charge surface, hydrogen binding surface, hydrophobic surface, ionizability surface, and solvent accessible surface (SAS) the interaction site. The depiction of the aromatic surface holds significance in the domain of molecular modeling, drug design, and structural analysis, as it facilitates the identification of plausible binding sites, comprehension of molecular recognition mechanisms, and anticipation of molecular interactions with other substances. Its utility is especially pronounced in investigations concerning interactions featuring aromatic rings, known to exert pivotal influences in diverse biological and chemical processes [40]. In this investigation, the presentation of the aromatic face

and edge surfaces is illustrated in Figure 7(a), represented by the colors orange and blue, respectively. A representation of the hydrogen bond surface as represented in Figure 7(c), serves as a visual elucidation of hydrogen bond interactions within a molecular framework. This graphical depiction employs a color-coded scheme to highlight amino acid residues engaged in hydrogen bonding, where the hydrogen atom acceptor sites are delineated in green, and the donor sites are portrayed in pink. Connecting lines or dashed lines between these regions denote the presence of hydrogen bonds, with the color scheme accentuating the respective donor and acceptor roles. The presented figure provides a lucid portrayal of the hydrogen bond pattern, emphasizing the specific involvement of amino acid residues in these interactions [41]. An illustration of the hydrophobicity surface (Figures 7(d) serve as a visual portrayal of hydrophobic regions inherent in a molecular configuration. Conventionally, hydrophobic zones are delineated by shades of blue, while hydrophilic areas maintain a neutral appearance or are represented in contrasting colors. Such depictions contribute to the comprehension of molecular interactions with water, as hydrophobic regions exhibit an aversion to water. The discerned hydrophobic surface of the receptor corroborates the presence of hydrophilic attributes surrounding the ligand. The representation of an ionization surface (Figure 7(e),) visually elucidates the acidic and basic attributes of a molecular surface. Within this portrayal, areas demonstrating a predilection for basic properties are depicted in blue, contrasting with regions inclined towards acidity, which are rendered in red [42-44]. The representation of the solvent accessible surface (SAS) (Figure 7(f)) delineates the surface area of a receptor accessible to a solvent, a pivotal parameter in the comprehension of molecular interactions. Within this graphical depiction, regions characterized by limited accessibility are portrayed in green, signifying areas less amenable to solvent interaction. Conversely, areas with heightened accessibility are rendered in blue, with a specific emphasis on polar region [42]. This visual representation aids in pinpointing specific regions where molecules can interact with the surrounding solvent [43].

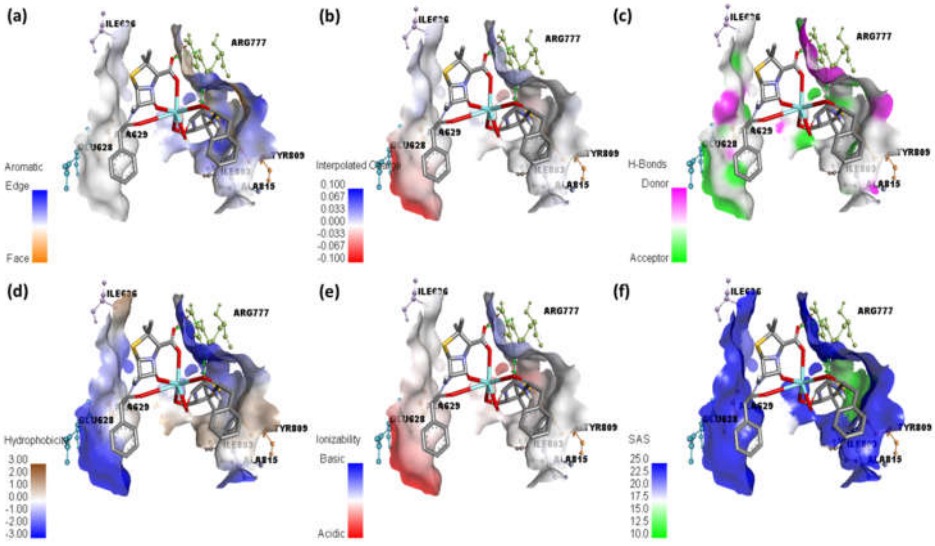

Figure 7. Representation of (a) aromatic surface, (b) Interpolated charge surface, (c) hydrogen binding, (d) hydrophobic surface, (e) ionizability surface, and (f) solvent accessible surface; between CSF1R and $Y(Pin)_2$ complex.

ACKNOWLEDGEMENTS

Princess Nourah bint Abdulrahman University Researchers Supporting Project number (PNURSP2024R75), Princess Nourah bint Abdulrahman University, Riyadh, Saudi Arabia.

CONCLUSION

The association and characterization of synthesized four different penicillinate complexes of yttrium(III), germanium(IV), tungsten(VI), and silicon within the temperature range of 25-800 ºC were delineated using spectral and analytical data. Theoretical data acquired through Density Functional Theory (DFT) calculations have played a pivotal role in elucidating the molecular geometry. Examination of the band gap energies for both the free penicillin potassium salt (Pin) drug and its penicillinate complexes [$Y(Pin)_2$ complex, $Ge(Pin)_2$ complex, $W(Pin)_2$ complex, and $Si(Pin)_2$ complex] reveals the heightened stability of the $Y(Pin)_2$ complex. These DFT-derived molecular parameters furnish valuable insights for prospective research endeavors. Molecular docking investigations indicate that all penicillinate complexes exhibit enhanced interactions with both the kinases - CSF1R (PDB ID: 7MFC) and MEK2 (PDB ID: 1S9I) associated with breast cancer progression and estrogen-dependent breast cancer, in comparison to the Pin drug alone. Notably, the $Y(Pin)_2$ complex demonstrates a particularly robust affinity for CSF1R, as evidenced by the highest binding energy value. Surface binding studies further corroborate the superior interaction of the $Y(Pin)_2$ complex with these receptors when juxtaposed with the unbound Pin drug.

REFERENCES

1. Anacona, J.R.; Calvo, J; Almanza, O.A. Synthesis, spectroscopic, and magnetic studies of mono-and polynuclear Schiff base metal complexes containing salicylidene-cefotaxime. *Int. J. Inorg. Chem*. **2013**, 2013, 108740.
2. Har, D.; Solensky, R. Penicillin and beta-lactam hypersensitivity. *Immunol. Allergy Clin. North Am.* **2017**, 37, 643-662.
3. Weiss, A.; Fallab, S; Erlenmeyer, H. Über das Komplexbildungsvermögen von Penicillin. *Helv. Chim. Acta*. **1957**, 40, 611-614.
4. Gutierrez, P.; Martinez, P.; Mayo, L.; Marquez A. Pivampicillin and penicillin-V complexes with Cu(II) in methanolic medium. *Afinidad* **1991**, 48, 61-65.
5. Martinez, J.H.; Martinez, P.J.; Gutierrez, P.; Martinez, M.I. Study of the reaction of complexation of penicillin V with cobalt(II) in methanolic medium. *Talanta* **1992**, 39, 637-641.
6. Asso, M.; Panossian, R.; Guiliano, M. Iron(II) complex of benzylpenicillin, synthesis and infrared structural characterisation. *Spectroscopy Lett*. **1984**, 17, 271-278.
7. Anacona, J.R.; Figueroa, E.M. Synthesis and characterization of metal complexes with penicillin. *J. Coord. Chem*. **1999**, 48, 181-189.
8. Grochowski, T.; Samochocka, K. Structural characterization of the platinum(II)-penicillin complexes. *Polyhedron* **1991**, 10, 1473-1477.
9. Dehghani, M.H.; Ahmadi, S.; Ghosh, S.; Khan, M.S.; Othmani, A.; Khanday, W.A.; Gökkuş, Ö.; Osagie, C.; Ahmaruzzaman, M.; Mishra, S.R; Lima, E.C. Sustainable remediation technologies for removal of pesticides as organic micro-pollutants from water environments: A review. *Appl. Surf. Sci. Advan*. **2024**, 19, 100558.
10. El-Habeeb, A.A.; Refat, M.S. Synthesis and Spectroscopic investigations of four new Y(III), Ge(IV), W(VI) and Si(IV) penicillin antibiotic drug complexes. *Spectrosc. Spect. Anal*. **2019**, 39, 2982-2988.

11. Khan, I.M.; Khan, A.; Shakya, S.; Osama, M.; Islam, M.; Naaz, F.; Ahmad, M. Investigating the binding of organic charge transfer co-crystals to human serum albumin by experimental and theoretical methods: Spectroscopy, molecular docking and DFT/TD-DFT studies. *New J. Chem*., **2024**, 48, 2527-2546.
12. Cicenas, J.; Zalyte, E.; Bairoch, A.; Gaudet, P. Kinases and cancer. *Cancers* **2018**, 10, 63.
13. Devasia, J.; Chinnam, S.; Khatana, K.; Shakya, S.; Joy, F.; Rudrapal, M.; Nizam, A. Synthesis, DFT and in silico anti-Covid evaluation of novel tetrazole analogues. *Polycycl. Aromat. Comp.* **2023**, 43, 1941-1956.
14. Hariharan, P.C.; Pople, J.A. The effect of d-functions on molecular orbital energies for hydrocarbons. *Chem. Phys. Lett*. **1972**, 16, 217-219.
15. Thompson, K.H.; Tsukada, Y.; Xu, Z.; Battell, M.; McNeill, J.H.; Orvig, C. Influence of chelation and oxidation state on vanadium bioavailability, and their effects on tissue concentrations of zinc, copper, and iron. *Biol. Trace Elem. Res*. **2002**, 86, 31-44.
16. O'Boyle, N.M.; Banck, M.; James, C.A.; Morley, C.; Vandermeersch, T.; Hutchison, G.R. Open Babel: An open chemical toolbox. *J. Cheminformatics* **2011**, 3, 33.
17. Dallakyan, S. PyRx-python prescription v. 0.8. The Scripps Research Institute, **2008**, 2010.
18. Chu, C.H.; Li, K.M.; Lin, S.W.; Chang, M.D.T.; Jiang, T.Y.; Sun, Y.J. Crystal structures of starch binding domain from *Rhizopus oryzae glucoamylase* in complex with isomaltooligosaccharide: Insights into polysaccharide binding mechanism of CBM21 family. *Proteins: Struct. Funct. Bioinformat.* **2014**, 82, 1079-1085.
19. Rehman, M.T.; AlAjmi, M.F.; Hussain, A. Natural compounds as inhibitors of SARS-CoV-2 main protease (3CLpro): A molecular docking and simulation approach to combat COVID-19. *Curr. Pharm. Des*. **2021**, 27, 3577-3589.
20. Eberhardt, J.; Santos-Martins, D.; Tillack, A.F.; Forli, S. AutoDock Vina 1.2.0: New docking methods, expanded force field, and python bindings. *J. Chem. Inf. Mode* **2021**, 61, 3891–3898.
21. Jeong, K.J.; Bae, D.S. Synthesis and characterization of Y_2O_3 powders by a modified solvothermal process. *Kor. J. Mater. Res*. **2012**, 22, 78-81.
22. Gu, Z.; Liu, F.; Howe, J.Y.; Paranthaman, M.P.; Pan, Z. Germanium-catalyzed hierarchical Al_2O_3 and SiO_2 nanowire bunch arrays. *Nanoscale* **2009**, 1, 347-354.
23. Chiu, H.W.; Chervin, C.N.; Kauzlarich, S.M. Phase changes in Ge nanoparticles. *Chem. Mater*. **2005**, 17, 4858-4864.
24. Akira, K.; Jagos, P. Microstructure and hardness of tungsten coating for high hest resistant material produced by means of gas tunnel type plasma spraying. *Trans. JWRI* **2009**, 38, 57-62.
25. Klug, H.P.; Alexander, L.E. *X-Ray Diffraction Procedures: For Polycrystalline and Amorphous Materials*, Wiley: New York; **1974**,
26. Al-Hazmi, G.H.; Hassanien, A.M.; Atta, A.A.; Refat, M.S.; Saad, H.A.; Shakya, S.; Adam, A.M.A. Supramolecular charge-transfer complex generated by the interaction between tinII) 2,3-naphtalocyanine as a donor with DDQ as an acceptor: Spectroscopic studies in solution state and theoretical calculations. *J. Mol. Liq*. **2022**, 362, 119757.
27. Shakya, S.; Khan, I.M.; Ahmad, M. Charge transfer complex based real-time colorimetric chemosensor for rapid recognition of dinitrobenzene and discriminative detection of Fe^{2+} ions in aqueous media and human hemoglobin. *J. Photochem. Photobiol. A*. **2020**, 392, 112402.
28. Islam, M.R.; Shakya, S.; Selim, A.; Alam, M.S.; Ali, M. Solvatochromic absorbance and fluorescence probe behavior within ionic liquid + γ-butyrolactone mixture. *J. Chem. Eng. Data* **2019**, 64, 4169-4180.
29. Yu, W.; He, X.; Vanommeslaeghe, K.; MacKerell, A.D., Jr. Extension of the CHARMM general force field to sulfonylcontaining compounds and its utility in biomolecular simulations. *J. Comput. Chem*. **2012**, 33, 2451-2468.
30. Foresman, J.B. in *Exploring Chemistry with Electronic Structure Methods: A Guide to Using Gaussian*, Frisch, E. (Ed.), Gaussian Inc.: Pittsburg, PA; **1996**.

31. Murugavel, S.; Ravikumar, C.; Jaabil, G.; Alagusundaram, P. Synthesis, crystal structure analysis, spectral investigations (NMR, FT-IR, UV), DFT calculations, ADMET studies, molecular docking and anticancer activity of 2-(1-benzyl-5-methyl-1H-1,2,3-triazol-4-yl)-4-(2-chlorophenyl)-6-methoxypyridine–a novel potent human topoisomerase IIα inhibitor. *J. Mol. Struct*. **2019**, 1176, 729-742.
32. Khan, I.M.; Shakya, S. Exploring colorimetric real-time sensing behavior of a newly designed CT complex toward nitrobenzene and Co^{2+}: Spectrophotometric, DFT/BarCS-DFT, and mechanistic insights. *ACS Omega* **2019**, 4, 9983-9995.
33. Hasan, A.H.; Shakya, S.; Hussain, F.H.; Murugesan, S.; Chander, S.; Pratama, M.R.F.; Jamil, S.; Das, B.; Biswas, S.; Jamalis, J. Design, synthesis, anti-acetylcholinesterase evaluation and molecular modelling studies of novel coumarin-chalcone hybrids. *J. Biomol. Struct. Dynam*. **2023**, 41, 11450-11462.
34. Bourzikat, O.; El Abbouchi, A.; Ghammaz, H.; El Brahmi, N.; El Fahime, E.; Paris, A.l.; El Kazzouli, S. Synthesis, anticancer activities and molecular docking studies of a novel class of 2-phenyl-5,6,7,8-tetrahydroimidazo [1,2-b] pyridazine derivatives bearing sulfonamides. *Molecules* **2022**, 27, 5238.
35. Tan, M.; Yu, D. *Molecular Mechanisms of ErbB2-Mediated Breast Cancer Chemoresistance. In Breast Cancer Chemosensitivity. Advances in Experimental Medicine and Biology*, Yu, D., Hung, M.C. (Eds.), Springer: New York; **2007**, 608, 119.
36. Richardsen, E.; Uglehus, R.D.; Johnsen, S.H.; Busund, L.-T. Macrophage-colony stimulating factor (CSF1) predicts breast cancer progression and mortality. *Anticancer Res*. **2015**, 35, 865-874.
37. Liu, D.; Zhou, K. BRAF/MEK pathway is associated with breast cancer in ER-dependent mode and improves ER status-based cancer recurrence prediction. *Clin. Breast Cancer* **2020**, 20, 41-50.
38. Akram, M.; Lal, H.; Shakya, S.; Kabir-ud-Din. Multispectroscopic and computational analysis insight into the interaction of cationic diester-bonded gemini surfactants with serine protease α-chymotrypsin. *ACS Omega* **2020**, 5, 3624-3637.
39. Khan, I.M.; Shakya, S.; Islam, M.; Khan, S.; Najnin, H. Synthesis and spectrophotometric studies of CT complex between 1,2-dimethylimidazole and picric acid in different polar solvents: exploring antimicrobial activities and molecular (DNA) docking. *Phys. Chem. Liq*. **2021**, 59, 753-769.
40. Islam, M.; Khan, I.M.; Shakya, S.; Alam, N. Design, synthesis, characterizing and DFT calculations of a binary CT complex co-crystal of bioactive moieties in different polar solvents to investigate its pharmacological activity. *J. Biomol. Struct. Dynam*. **2023**, 41, 10813-10829.
41. Alsanie, W.F.; Alamri, A.S.; Alyami, H.; Alhomrani, M.; Shakya, S.; Habeeballah, H.; Alkhatabi, H.A.; Felimban, R.I.; Alzahrani, A.S.; Alhabeeb, A.A.; Raafat, B.M. Increasing the efficacy of seproxetine as an antidepressant using charge–transfer complexes. *Molecules* **2022**, 27, 3290.
42. Ranjbar, A.; Jamshidi, M.; Torabi, S. Molecular modelling of the antiviral action of Resveratrol derivatives against the activity of two novel SARS CoV-2 and 2019-nCoV receptors. *Eur. Rev. Med. Pharmacol. Sci*. **2020**, 24, 7834-7844.
43. Hussen, N.H.; Hasan, A.H.; Jamalis, J.; Shakya, S.; Chander, S.; Kharkwal, H.; Murugesan, S.; Bastikar, V.A.; Gupta, P.P. Potential inhibitory activity of phytoconstituents against black fungus: In silico ADMET, molecular docking and MD simulation studies. *Comput. Toxicol.* **2022**, 24, 100247.